
Latent Variable Sequence Identification for Cognitive Models with Neural Bayes Estimation

Ti-Fen Pan¹
tfpan@berkeley.edu

Jing-Jing Li¹
jl3676@berkeley.edu

Bill Thompson²
wdt@berkeley.edu

Anne Collins^{1,2}
annecollins@berkeley.edu

¹Helen Wills Neuroscience Institute, University of California, Berkeley, Berkeley, CA, USA

²Department of Psychology, University of California, Berkeley, Berkeley, CA, USA

Abstract

Extracting time-varying latent variables from computational cognitive models is a key step in model-based neural analysis, which aims to understand the neural correlates of cognitive processes. However, existing methods only allow researchers to infer latent variables that explain subjects' behavior in a relatively small class of cognitive models. For example, a broad class of relevant cognitive models with analytically intractable likelihood is currently out of reach from standard techniques, based on Maximum a Posteriori parameter estimation. Here, we present an approach that extends neural Bayes estimation to learn a direct mapping between experimental data and the targeted latent variable space using recurrent neural networks and simulated datasets. We show that our approach achieves competitive performance in inferring latent variable sequences in both tractable and intractable models. Furthermore, the approach is generalizable across different computational models and is adaptable for both continuous and discrete latent spaces. We then demonstrate its applicability in real world datasets. Our work underscores that combining recurrent neural networks and simulation-based inference to identify latent variable sequences can enable researchers to access a wider class of cognitive models for model-based neural analyses, and thus test a broader set of theories.

1 Introduction

Neuroscientists often use model-based neural analysis to explain how the brain supports cognition by relating neural activity to computational cognitive models' latent variables [13]. Model variables provide quantitative, trial-by-trial predictors of neural activity, allowing researchers to investigate the underlying neural implementation of computational cognitive processes and how they vary across individuals [26]. For instance, reward prediction errors (RPEs) extracted from a reinforcement learning (RL) model have been found to correlate with brain signals in the human ventral striatum under functional magnetic resonance imaging (fMRI) [35], as well as phasic activity of dopamine neurons in non-human animals [19]. The traditional method for extracting time-varying latent variables from experimental data consists of two steps [45]: first, identify the best-fitting model parameters. Second, infer the latent variables by running the computational model off-policy over participants' experienced sequences of stimuli and actions with the best-fitting model parameters. However, both steps limit the type of models that can be considered. In the first step, best-fitting parameters may be difficult to obtain in a large subspace of relevant cognitive models. Indeed,

researchers typically use likelihood-dependent methods like Maximum Likelihood Estimation (MLE) [33], Maximum a Posteriori (MAP) [14] or hierarchical Bayesian modeling [3]. Nonetheless, these methods fall short for models with analytically intractable likelihood [29]. In addition, some latent variables may be complex to infer even when best-fitting parameters are known [2]. Due to these limitations, researchers typically develop complex and customized statistical approaches that are not generalizable to broader computational models [18, 20].

Most computational models with intractable likelihoods can be simulated. As a result, simulation-based inference (SBI) methods have used this attribute to bypass the likelihood computation [9]. Specifically, SBI methods combined with artificial neural networks (ANN) have successfully enabled parameter recovery across a wide range of computational models because of ANN’s ability to handle high-dimensional data for amortized inference after training. These neural-based SBI methods are primarily based on Bayesian inference, aiming to approximate likelihood (neural likelihood estimation, NLE) [6] or the posterior (neural posterior estimation, NPE) [36] (see review [48]). Recently, the method of training neural networks to map data to parameter point estimates has shown promising avenues in a variety of applications [29, 39]. [40] conceptualized this method by connecting it to classic Bayes estimators, which we refer to as neural Bayes estimators.

However, time-varying latent variable extraction in likelihood intractable models is still under-explored [41]. The existing SBI methods are primarily concerned with parameter recovery or model identification. Though the SBI methods help recover the model parameters, it may be difficult to derive underlying latent variable sequences given recovered parameters, specifically when the latent variables have sequential dependencies. Moreover, the existing neural-based SBI methods are still crippled by highly parameterized computational models. The computational cost increases exponentially fast with the number of parameters, especially the models with non-orthogonal parameterizations [40].

Here, we propose an approach which aims to identify **Latent variable Sequences** with ANNs, which we call "LaseNet". LaseNet is built upon neural Bayes estimators, given their success in applying to computational cognitive models with sequential dependencies and intractable likelihoods [37]. We use simulated datasets to train an ANN, which learns a direct mapping between a sequence of observable variables (e.g., the participant’s actions or received outcomes) and the targeted latent variable space (e.g., the participant’s reward expectation, or subjective rule choice). We first outline the problem formalism and cognitive models in section 2, then introduce the method in section 3. In section 4, we show that LaseNet infers time-varying latent variables that are close to synthetic ground truth for a variety of computational cognitive models and task environments, especially when the models are highly parameterized or intractable. We showcase LaseNet’s real-world applicability in section 5: using experimental data from a real mice dataset, our approach successfully infers both discrete and continuous latent variables compared to likelihood-dependent estimations. Finally, we discuss related work, and the benefits and limitations of LaseNet.

2 Preliminaries

Problem formulation Suppose that there is a latent variable model that produces a time-series of observable variables $Y = (y_1, y_2 \dots y_T)$ and unobservable latent variables $Z = (z_1, z_2 \dots z_T)$ given a set of model parameters θ , where T denotes the number of trials. We can then describe the generation process for the time-varying latent variables as follows:

$$z_t \sim f(z_{t-1}, \bar{y}_{t-1}, \theta_f), \quad y_t \sim g(z_t, \theta_g) \tag{1}$$

where f and g are both density functions parameterized by θ_f and θ_g respectively, \bar{y}_{t-1} corresponds to the history of Y up to the trial t . Our goal is to infer the unobservable latent variables Z at each time point given variables Y . Therefore, our objective can be described as:

$$\tilde{Z} = \arg \max_{Z \in K} P(Z | Y) \tag{2}$$

where K denotes the possible values in the latent variable space. Note that we do not assume Markovian property in the latent variable model and will demonstrate how LaseNet can apply to cognitive models with and without Markovian property.

Task environments and computational cognitive models We consider representative learning and decision-making tasks from the cognitive literature. Biological agents (e.g., humans, mice)

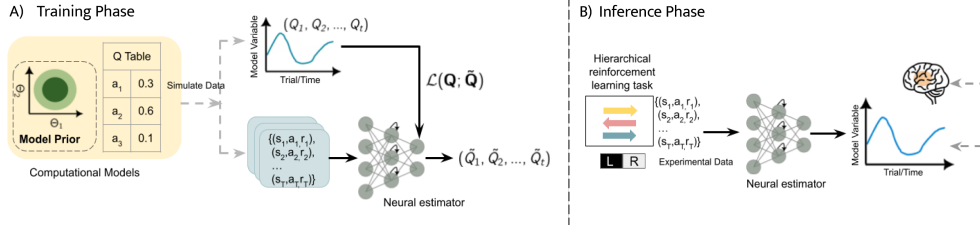


Figure 1: **Schematic of LaseNet method:** (A) The network is trained with a simulated dataset to predict time-varying latent variables derived from a computational cognitive model (e.g., the chosen Q-values). The input may include a time-series of simulated stimuli, actions, and rewards. Corresponding model variables are used as training targets. (B) At inference time, the trained network predicts the latent variables for experimental data from biological agents where ground truth is unknown. The extracted latent variables are commonly used in relating behavior to brain signals.

are assumed to be in a state that is represented by the stimulus presented (which can be either images, or parameterized along a feature dimension such as the orientation of a grating); to make a discrete choice (such as pressing one of two keys or levers); and to observe some feedback (e.g., points for humans, water reward for mice). Computational cognitive models are simple algorithms with few parameters (typically < 10) which instantiate hypotheses about information flow and provide quantitative predictions about behavioral and neural data. We use representative cognitive models based on tabular reinforcement learning (RL) models and hidden Markov models (HMM). [34, 17, 18, 10]. In the RL model family, we use Q-learning based cognitive models, which assumes that a participant tracks the Q-value of each state and action, and uses these Q-values to inform the action selection on each trial. After each trial’s outcome, the model updates Q-values by first computing the RPE, denoted by δ , as the discrepancy between the expected and the observed values, and then adjusting the Q-value of the chosen action a with RPE scaled by a learning rate α [44]:

$$\begin{aligned} \delta_t &= r_t - Q_t(a_t) \\ Q_{t+1}(a_t) &= Q_t(a_t) + \alpha \delta_t \end{aligned} \quad (3)$$

One goal is to infer time-varying Q-values \mathbf{Z} given observable rewards, stimuli and actions \mathbf{Y} . We also explore model extensions with target outputs that include additional discrete latent states. In HMM, we use a cognitive model based on the Bernoulli generalized linear model (GLM) observations (GLM-HMM). Our example target output is the HMM hidden states \mathbf{Z} given rewards/stimuli and actions \mathbf{Y} . See Appendix B for more detailed descriptions of the cognitive models.

3 Neural SBI for Time-Varying Latent Variables

3.1 SBI with neural networks

Our proposed method, like standard SBI methods combining neural networks, consists of two phases: training and inference (Fig. 1). During the training phase, we create a synthetic dataset by simulating the targeted computational cognitive model on the target experimental task. LaseNet is trained using model-simulated observable data \mathbf{Y} as input and a series of model-derived latent variables \mathbf{Z} as output. During the inference phase, the trained LaseNet takes the observable experimental data as input to infer a sequence of unobservable latent variables.

3.2 Neural Bayes estimators

Our method extends neural Bayes estimators that learn a mapping between data and parameter point estimates. The neural estimators can be constructed within a decision-theoretic framework [4]. Consider a loss function $\mathcal{L}(z_t; \tilde{z}_t(\mathbf{y}))$, which assesses an estimator $\tilde{z}_t(\cdot)$ for a given z_t and dataset $\mathbf{y} \sim f(\mathbf{y} | \theta)$, where $f(\cdot)$ is the density function conditioned on model parameters. The estimator risk is defined as the loss averaged across all possible data realizations, that is:

$$R(\tilde{z}_t(\cdot)) = \int_{\mathbf{y}} \mathcal{L}(z_t, \tilde{z}_t(\mathbf{y})) f(\mathbf{y} | \theta) d\mathbf{y} \quad (4)$$

A minimizer of the expected risk $R(\tilde{z}_t^*)$ weighted by model priors $p(\theta)$ is said to be a Bayes estimator. We formalize the neural networks trained to minimize the loss function given by:

$$\gamma^* = \arg \max_{\gamma} \sum_{n=1}^N \sum_{t=1}^T \mathcal{L}(z_t^n, \tilde{z}_t^n(\mathbf{y})) \quad (5)$$

where γ are the neural network parameters, N is the number of samples, and T is the number of time points in the dataset.

3.3 Network architecture

LaseNet aims to learn a mapping between observable variable space \mathbf{Y} and latent variable space Z . To learn this relationship, the structure of LaseNet is composed of two components: bidirectional recurrent neural network (bi-RNN) layer [42] followed by Multilayer Perceptrons (MLPs).

The building blocks of bi-RNN is Gated Recurrent Units (GRU) [11]. Bidirectionality enables the network to learn embeddings from both past and future history. A summary embedding S is yielded by concatenating the past and future embeddings. We can represent the learned summary S at each time point y_t as:

$$S(y_t) = \left\langle \overrightarrow{\psi}(\{y\}_{i=1}^t), \overleftarrow{\psi}(\{y\}_{i=t}^T) \right\rangle \quad (6)$$

where function $\overrightarrow{\psi}$ (forward pass), $\overleftarrow{\psi}$ (backward pass) transform a time series $(y_1, y_2 \dots y_T)$ to a lower dimensional embedding space. Following the bi-RNN, MLPs map the summary embeddings to the targeted latent variable space. Let ϕ denote a universal function approximator. We can describe the estimated latent variable for each time point as $\tilde{z}_t = \phi(S(y_t))$. When training LaseNet, the main objective is to find a set of neural network parameters (i.e., weights or biases) that minimizes the loss between true and estimated latent variables: $\mathcal{L}(\mathbf{z}; \tilde{\mathbf{z}})$ as Eq. 5.

Output layers By changing the output layers, our architecture is adaptable to both continuous and discrete latent variables. For continuous latent space, we used a linear activation with mean-squared error (MSE) loss. For discrete latent space, we used a softmax activation function in the output layer, with a cross-entropy loss. To predict both types of latent spaces at once, we added two output layers for each types after the MLP layers. See Appendix C for the details of the architectures and network training.

4 Experiments in Synthetic Dataset

4.1 Experimental settings

Cognitive models and tasks We evaluated LaseNet against four computational cognitive models and task environments. We first evaluated with two tractable models that afford a comparison to existing techniques: 4-parameter reinforcement learning model (**4-P RL**)[49], and a meta reinforcement learning model with dynamic noise (**Meta RL**)[30]. We tested both cognitive models performing on a two-armed bandit with probabilistic reversal task. We then validated LaseNet in two intractable models: a 3-states **GLM-HMM** [2] performing on a perceptual decision making task (for which a custom statistical inference exists, providing a benchmark) and a hierarchical reinforcement learning model (**HRL**) with a novel dynamic decision making task [37], for which no benchmark method exists. In this dynamic decision making task, a participant observes 3 arrows (in 3 different colors), each pointing at either left or right direction as depicted in the inference task Fig. 1B. The participant selects an action that corresponds to either left or right side in order to get rewarded. The correct arrow changes unpredictably in the task, which means that the participant must keep track of which arrow currently indicates the rule to follow. This task structure is hierarchical because the choice policy (left/right) depends on the higher-level rule (color) participant choose to follow; participants' internal "arrow rule" choice is unobservable and one of the targets of latent variable estimation. See Appendix Table 1 for the summary of cognitive models.

Dataset For each LaseNet estimators, we simulated at most 9000 pairs of (\mathbf{Z}, \mathbf{Y}) with 720 trials in each pair as training data (representing a standard cognitive task duration for a real biological participant). We hold out 10% of training data as the validation set to fine-tune the hyperparameters.

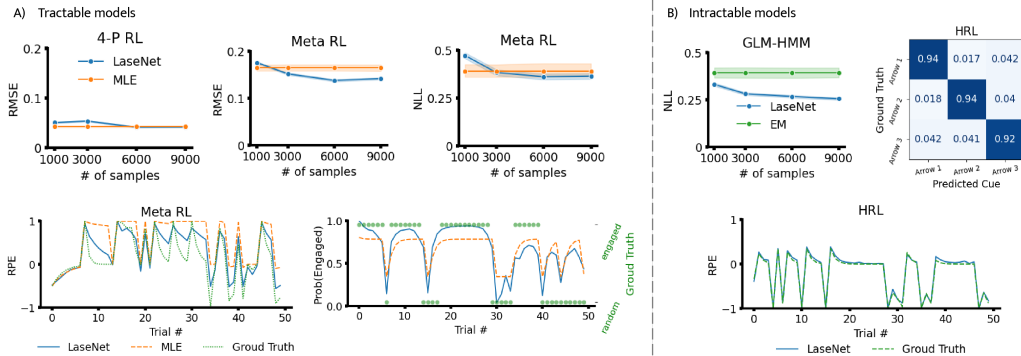


Figure 2: **Performance on synthetic dataset.** (A) In tractable models, LaseNet identifies continuous (Q-values) and discrete (engaged vs. random) latent variables with comparable precision but less variance (less shaded area) than MLE. Example time series plots (bottom row) are based on one simulated participant from the Meta-RL model. Results show strong agreement between MLE and LaseNet. Note that the reward prediction error (RPE) is obtained by subtracting estimated Q values from rewards. (B) In the GLM-HMM model, LaseNet outperforms EM even with fewer training samples. In HRL, LaseNet has high accuracy in inferring the unobservable chosen rule and RPE.

We simulated additional unseen 1000 pairs of (\mathbf{Z}, \mathbf{Y}) with 720 trials as testing data. Except for prior misspecified evaluation, each (\mathbf{Z}, \mathbf{Y}) pair was generated based on model parameters θ drawn from uniform priors.

Other estimators As a comparison against LaseNet that targets latent variables identification, we also tested commonly used likelihood dependant estimators such as MAP or MLE on the same dataset [45]. Two steps are required for researchers to recover latent variables with likelihood dependant estimators. The first step is to find the best fitting model parameters θ given observable data \mathbf{Y} by either maximizing a likelihood function $P(\mathbf{Y} | \theta)$ or posterior probability $P(\mathbf{Y} | \theta) P(\theta)$. At the second step, we used the best fitting parameters $\hat{\theta}$ and observable data \mathbf{Y} to derive the latent variables \mathbf{Z} , where \mathbf{Z} can be in a discrete or continuous space. We then approximate latent variables from the targeted models with $\hat{\theta}$ and \mathbf{Y} as input: $\tilde{\mathbf{Z}} \approx \mathbf{f}(\mathbf{Y}; \hat{\theta})$, where \mathbf{f} is either an extended RL algorithm or the GLM-HMM function. See Appendix C.3 for more detailed descriptions of the methods.

Metrics For the metrics in Fig. 2, Fig. 3, and Fig 4, results were averaged across trials, where marker and error bars represent mean and 2 standard deviation over all test samples. See Appendix C.2 for more detailed evaluation metrics.

4.2 Tractable models

We examined LaseNet with synthetic datasets generated from two tractable models: 4-P RL and Meta RL. The input data are a time-series of observable rewards and actions.

4-P RL The 4P-RL model is simulated in a 2-choice probabilistic reversal learning environment and follows the same Q-value update described in 2 with minor variants that bring it closer to human behavior [49]; the policy is a softmax over Q-values: $P(a_i) \propto \exp(\beta Q(a_i))$, with inverse temperature β controlling noise in the policy. Our target latent variable is the chosen Q-values, representing the subjective reward expectation at each trial. We found LaseNet reaches similar average RMSE (0.041) to a standard MLE-based approach (0.042) (Fig. 2A), showing our approach’s capability to recover latent variables in a simple model and environment. We next tested it in a more complex cognitive model, where we can infer both continuous and discrete latent variables.

Meta RL Meta RL with dynamic noise model shares the similar Q-value update policy as 4-P RL. The major difference is that the Meta RL model assumes a participant has two latent attentive states: engaged and random. The transition from one latent state to the other is controlled by a hidden

Markov process [30]. Attentive states are characterized by two different policies:

$$P(a) \propto \begin{cases} 1/n & \text{if state=random} \\ \exp(\beta Q_t) & \text{if state=engaged} \end{cases}$$

where n denotes the number of actions and softmax β controls how deterministic the choices are. Two time-varying latent variables are inferred here: chosen Q-values (continuous latent space) and two attentive states (discrete latent space). We found that the RMSE of LaseNet is lower with less variance compared to MLE (Fig. 2A), after training with 6k simulated participants. Moreover, in identifying attentive states, we calculated a negative log likelihood (NLL) across simulated participants. LaseNet had a slightly lower (better) NLL than MLE. (Fig. 2A), which may be due to parameter recovery issues with MLE (detailed in Appendix C.3.1). LaseNet is less affected by the highly parameterized models because we learn a mapping from the observable variable space to latent variable space without conditioning on the model parameters.

4.3 Intractable models

Finally, we evaluated LaseNet with two intractable models: HRL and GLM-HMM. Other than rewards and actions, we also included a time-series of stimuli (left/right arrow directions for HRL; the rotation angles of visual stimuli for GLM-HMM) as input data for LaseNet. In the case of GLM-HMM, an approximate statistical inference method exists, providing a benchmark to compare our approach. In the case of HRL, we show that LaseNet also works well in a situation where no approximation is available, showing the breadth of applicability of LaseNet.

GLM-HMM In a mice perceptual decision-making task environment, we used a 3-state GLM-HMM that can capture three attentive states: engaged, biased-left, and biased-right [2]. The model containing 3 independent Bernoulli GLMs conditioned by the participant’s current latent attentive state, each defined by a weight vector specifying how inputs are integrated into a policy in that particular state. The probability of a leftward choice ($y_t = 0$) given the input vector x_t and the latent state z_t is given by

$$p(y_t = 0 \mid x_t, z_t = k) = \frac{1}{1 + e^{-x_t \cdot w_k}} \tag{7}$$

where $w_k \in \mathbb{R}_4$ denotes the GLM weights for latent state $k \in \{1, 2, 3\}$. We trained LaseNet to predict time-varying attentive states. We used approximate expectation–maximization (EM) algorithm as our benchmark technique [18, 2]. Specifically, the expectation step is solved by the standard forward-backward algorithm for HMMs. Fig. We found that the average NLL value of LaseNet (0.255) is much lower than EM (0.392), implying that LaseNet had higher precision in predicting state probability (Fig. 2B).

HRL Instead of tracking the Q-values of observable actions, the HRL model assumes that a participant tracks the value of each arrow, and chooses between the arrows noisily: $P(\text{arrow}) \propto \exp(\beta Q_t(\text{arrow}))$. The arrow choice is unobservable as described in 4.1; observable left-right choice is then assumed to be ϵ -greedy conditioned on the selected arrow. Our target latent variables are chosen Q-values (continuous latent space indexing the value of the current arrow the participant is following) and the chosen arrow (discrete latent space). To our knowledge, no standard benchmark method exists for inferring the latent variables of interest. Nonetheless, compared to the ground truth, LaseNet reaches 93% accuracy in latent discrete cue identification (arrow selection) and the RMSE across agents is 0.119 in Q-values identification (2B). Note that we determined the predicted cue by taking the cue with the highest probability from the neural estimator’s output.

4.4 Prior misspecification

We examined the impact of misspecified priors between LaseNet and the likelihood dependent methods in one tractable (4-P RL) and one intractable (GLM-HMM) models. Overall, LaseNets trained with the dataset generated from a less biased model prior resulted in a more robust performance. All LaseNets for 4P-RL were trained with 22k simulated participants and with 9k simulated participants for the GLM-HMM.

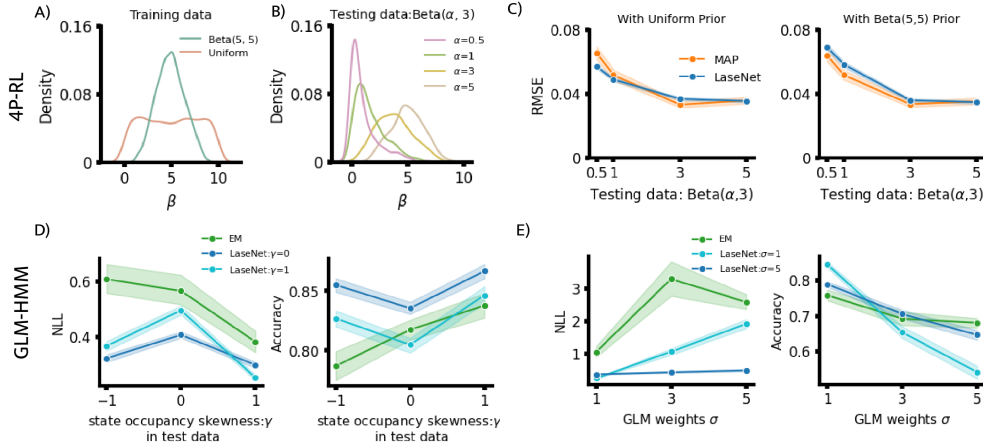


Figure 3: **Performance on misspecified priors.** Top row shows the impact of training with misspecified prior of model parameter β in a 4-P RL model. (A) We compared two LaseNets trained with different prior distributions: a beta distribution and a uniform distribution. (B) Four test datasets generated from four different distributions of parameter β are evaluated. (C) Training with a uniform distribution has more robust performance across different test datasets; Bottom row summarizes the impact of training with misspecified priors in a GLM-HMM model. (D) Three latent state distributions with positive (+1), no (0), and negative (-1) skewness γ are evaluated. LaseNet trained with a uniform distribution (no skewness) outperforms both LaseNet trained with positive skewness and EM here. (E) Adjusting the σ (noise level) in GLM weights in GLM-HMM models reveals that LaseNet is more robust when trained with noisier dataset (i.e., higher σ).

4P-RL Softmax β parameter in 4-P RL controls the randomness of a participant’s action: higher beta results in a more deterministic actions. We evaluated two priors of β : a Beta ($\alpha=5, \beta=5$) prior (green line in Fig. 3A) and a uniform prior within an empirical range (orange line in Fig. 3A). We trained two LaseNet estimators with dataset generated from these two priors respectively. We tested the performance of LaseNet and MAP estimators with four different β priors (red, light green, yellow and brown lines in Fig. 3B). We found that the LaseNet trained with a uniform prior had lower RMSE (0.044) across different β priors (Fig. 3C).

GLM-HMM Here, we changed the priors of the hidden state distribution (transitions matrix) and GLM weights, independently. In state distribution, we tested three skewness γ levels: positive (1), negative (-1) and no (0) skewness. No skewness means that each state occupancy are equal (i.e., uniform distribution). We examined two LaseNet estimators: one is trained with positive skewness and the other is with no skewness in comparison with EM having a positive skewness prior. We showed that LaseNet with equal states prior (no skewness) reaches the highest accuracy and lowest NLL among all (Fig. 3D). Furthermore, in changing the σ in the GLM weights with a fixed mean, we found that LaseNet trained with a higher σ (noisier) dataset is more robust (Fig. 3E). This suggests our approach is applicable even if there is no strong empirical priors.

5 LaseNet Infers Latent Variable Sequence in Real Data

We applied LaseNet to two real mice datasets: dynamic foraging dataset with Meta RL model (tractable) and decision making dataset with GLM-HMM model (intractable). The process of constructing LaseNet is described in section 3. See Appendix C.4 for more training details.

Meta RL inference in mice dynamic foraging dataset The dynamic foraging dataset consists of 48 mice data collected from [25]. Each mouse did a two-armed bandits task with dynamic reward schedules. We trained LaseNet to infer the latent attentive state (engaged vs random), Q values of left actions and right actions. In comparison, we adopted MLE with an estimated likelihood function described in [30] as a benchmark. We found that in estimating Q-values, LaseNet had similar result as MLE. However, in attentive state identification, MLE tends to estimate state probability with high

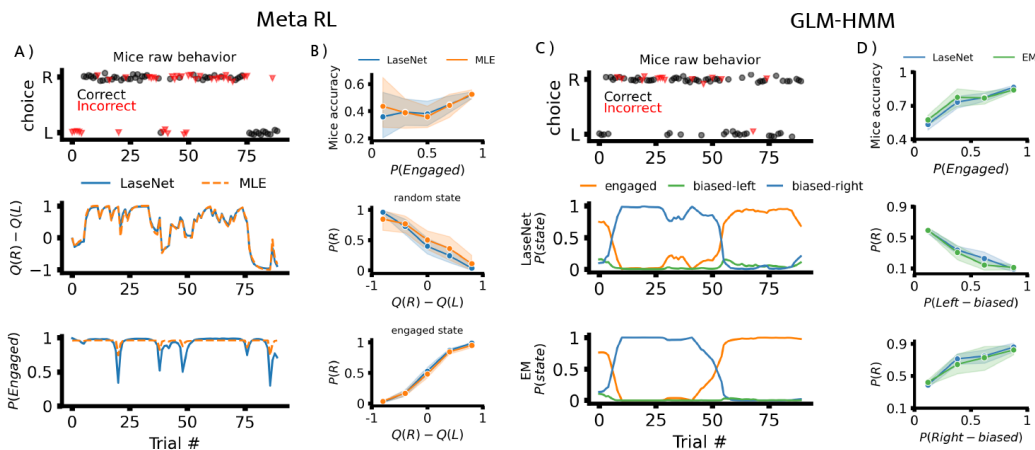


Figure 4: **Validation of LaseNet application on real mice data** (A) Top: raw behavioral data of one example mouse in the dynamic foraging dataset. Each dot represents a single trial; the y-axis indicates if the mouse went rightward or leftward on the trial. Middle: estimated Q-values difference. Bottom: latent engaged probability trial-by-trial in the example mouse. (B) LaseNet and MLE identify similar relationships between the mice response accuracy and probability of rightward choice given estimated latent variables. (C) Top: raw behavioral data of one mouse in IBL dataset. Middle and bottom rows: state probabilities from LaseNet and EM estimation, respectively, highlighting high agreement of certainty about the mouse’s internal state. (D) LaseNet and EM keep high consensus with the mice response accuracy and probability of rightward choice given different latent policy states.

certainty (Fig. 4A). In the behavioral analysis (Fig. 4B), we found a similar trend between LaseNet and MLE: mice exhibit higher response accuracy when estimated engaged state probability is higher, and the inferred policy (probability of right choice $P(R)$ as a function of $Q(R) - Q(L)$) is consistent with the inferred latent states, validating the model assumptions.

GLM-HMM inference in mice decision making dataset We used a mice decision making dataset published by the International Brain Laboratory (IBL) [27]. The dataset consists of 37 mice performing a visual detection decision making task developed in [8]. We extracted a time series of choice, reward and stimuli data from mice and fed into the trained LaseNet for inference. The LaseNet inferred time-varying probabilities for three HMM states (engaged, left-biased, right-biased). In comparison, we used EM fitting procedure described in [2] as a benchmark. We obtained similar results in predicting state probabilities between LaseNet and EM (Fig. 4C). Fig. 4D shows a high agreement between LaseNet and EM, the mean absolute difference is 0.027 in mice accuracy, and 0.037 in right choice probability.

6 Related Work

Our framework is inspired by a wide range of studies that used ANN and SBI to bypass likelihood computation and generally work intractable computational models [15, 36, 38]. Specifically, our work focuses on the approach of mapping data to variables point estimates using neural networks. The recent work [40] formalized the neural point estimation within a decision-theoretic framework. This neural point estimators date back to 12 and have shown promising results in a variety of fields, including spatio-temporal forecasting [47], spatial fields [23, 29] and time-series [37].

RNNs have been used widely in the processing of time-series data, which is a common data type in computational cognitive models. Several studies have adopted RNN-based models for interpreting behavioral data [16, 32]. Unlike prior research, which used RNN-based models as cognitive models, recent research has used RNNs for parameter recovery and model identification in computational cognitive models [37, 21, 22].

To our knowledge, two recent studies have employed a similar workflow to identify time-varying variables using neural networks and SBI. The first study uses superstatistics framework to recover the

dynamics of model parameters θ [41], which differs from our work in that our target is the derived latent variables. The second study focuses solely on HMMs and develops a neural estimator based on joint distribution of model parameters θ and hidden states [24]. Future work should compare these approaches directly on matched computational models and real dataset, as well as evaluate against various metrics for latent variable identification [31].

7 Discussion

We proposed a method, LaseNet, for learning a mapping between an observable data space and a targeted latent variable space using ANNs and synthetic data. In comparison to traditional statistical estimators such as MLE or EM, LaseNet can infer latent variables without requiring likelihood computation. Unlike standard neural point/posterior estimators, our goal is to identify the derived latent variable of a computational model rather than recover its parameters. Overall, LaseNet has some significant advantages over statistical estimators when fitting data to computational cognitive models:

First, we observed LaseNet exhibits comparable performance to statistical estimators in tractable models. Specifically, LaseNet is less susceptible to highly parameterized models (e.g., Meta RL), which are also more difficult to recover with standard neural estimators trained for parameter recovery [40]. Additionally, our developed network structure is adaptable to infer both continuous and discrete latent spaces, allowing training one network to identify both latent spaces simultaneously without performance degradation.

Furthermore, we showed LaseNet accurately identified latent variables in intractable models without the need for complex statistical estimators to approximate the likelihoods (e.g. approximate EM algorithm). It suggests that researchers can adopt our generic framework to fit a simple intractable model like HRL without developing customized statistical inference methods.

When training with a dataset derived from less informative model parameter priors, LaseNet becomes more robust to different prior distributions in the test. To achieve high performance, the networks do not require a large training sample (up to 22K). It implies that, in a real-world experimental setting, researchers can use LaseNet to fit experimental data without using strong empirical model parameter priors and high computational power. Lastly, in comparison to other statistical estimators, LaseNet showed its generalizability to identify latent variables in computational cognitive models (RL-based models without Markovian property and HMM-based models with Markovian property).

Though LaseNet is generalizable and flexible for various computational models, there are some limitations: First, similar to current statistical inference for cognitive modeling, LaseNet lacks uncertainty estimation. Consequently, LaseNet estimators are unable to detect out-of-distribution data. Uncertainty estimation is crucial because researchers may have misspecified models in a simulated dataset. In Appendix D.1, we showed how fitting a four-state GLM-HMM to a three-state GLM-HMM significantly reduces accuracy. Given the amortized nature of neural point estimators, bootstrapping is frequently used to quantify uncertainty. However, bootstrapping becomes computationally expensive in time-series prediction tasks. To mitigate this issue, one can perform a model identification first before training LaseNet or consider integrating with evidential learning [1, 43]; (See Appendix E for our experiments using evidential learning).

In addition, LaseNet does not provide underlying model parameters that are relevant to the targeted latent variables. Though LaseNet is less affected by highly parameterized models compared to estimators relying on model parameter recovery, it may be important for researchers to understand the relationship between the model parameters with resulting latent variables. As a result, parameter recovery with other neural-based estimators should be used in conjunction with LaseNet [37].

Finally, there is no ground truth for assessing the performance with the real data we used. We can only show comparable qualitative results between methods. Future work should consider using dataset that includes measurement for latent states (e.g., reaction time [7], pupil size [28]) and examine whether our proposed approach can outperform traditional statistical inference in real experimental settings.

8 Conclusion

Extended from neural Bayes estimation framework, we show that LaseNet performs well even when the likelihood of a computational model is intractable. LaseNet is adaptable to both discrete and continuous latent variable identification, as well as generalizable across different computational models. In conclusion, breaking down the barrier of intractable likelihood and recovering the latent dynamics of computational cognitive models will provide researchers with new insights into previously inaccessible relations between behavioral and neural data.

References

- [1] A. Amini, W. Schwarting, A. Soleimany, and D. Rus. Deep evidential regression. *Advances in Neural Information Processing Systems*, 33:14927–14937, 2020.
- [2] Z. C. Ashwood, N. A. Roy, I. R. Stone, I. B. Laboratory, A. E. Urai, A. K. Churchland, A. Pouget, and J. W. Pillow. Mice alternate between discrete strategies during perceptual decision-making. *Nature Neuroscience*, 25(2):201–212, 2022.
- [3] B. Baribault and A. G. Collins. Troubleshooting bayesian cognitive models. *Psychological Methods*, 2023.
- [4] R. L. Berger and G. Casella. *Statistical inference*. Duxbury, 2001.
- [5] J. Bergstra, D. Yamins, and D. Cox. Making a science of model search: Hyperparameter optimization in hundreds of dimensions for vision architectures. In *International conference on machine learning*, pages 115–123. PMLR, 2013.
- [6] J. Boelts, J.-M. Lueckmann, R. Gao, and J. H. Macke. Flexible and efficient simulation-based inference for models of decision-making. *Elife*, 11:e77220, 2022.
- [7] M. M. Botvinick, T. S. Braver, D. M. Barch, C. S. Carter, and J. D. Cohen. Conflict monitoring and cognitive control. *Psychological review*, 108(3):624, 2001.
- [8] C. P. Burgess, A. Lak, N. A. Steinmetz, P. Zatka-Haas, C. B. Reddy, E. A. Jacobs, J. F. Linden, J. J. Paton, A. Ranson, S. Schröder, et al. High-yield methods for accurate two-alternative visual psychophysics in head-fixed mice. *Cell reports*, 20(10):2513–2524, 2017.
- [9] G. Busetto Alberto, E. Numminen, J. Corander, M. Foll, C. Dessimoz, et al. Approximate bayesian computation. *PLoS computational biology*, 9(1), 2013.
- [10] A. J. Calhoun, J. W. Pillow, and M. Murthy. Unsupervised identification of the internal states that shape natural behavior. *Nature neuroscience*, 22(12):2040–2049, 2019.
- [11] K. Cho, B. Van Merriënboer, D. Bahdanau, and Y. Bengio. On the properties of neural machine translation: Encoder-decoder approaches. *arXiv preprint arXiv:1409.1259*, 2014.
- [12] K. H. Chon and R. J. Cohen. Linear and nonlinear arma model parameter estimation using an artificial neural network. *IEEE transactions on biomedical engineering*, 44(3):168–174, 1997.
- [13] J. D. Cohen, N. Daw, B. Engelhardt, U. Hasson, K. Li, Y. Niv, K. A. Norman, J. Pillow, P. J. Ramadge, N. B. Turk-Browne, et al. Computational approaches to fmri analysis. *Nature neuroscience*, 20(3):304–313, 2017.
- [14] D. Cousineau and S. Helie. Improving maximum likelihood estimation using prior probabilities: A tutorial on maximum a posteriori estimation and an examination of the weibull distribution. *Tutorials in Quantitative Methods for Psychology*, 9(2):61–71, 2013.
- [15] K. Cranmer, J. Brehmer, and G. Louppe. The frontier of simulation-based inference. *Proceedings of the National Academy of Sciences*, 117(48):30055–30062, 2020.
- [16] A. Dezfouli, H. Ashtiani, O. Ghattas, R. Nock, P. Dayan, and C. S. Ong. Disentangled behavioural representations. *Advances in neural information processing systems*, 32, 2019.
- [17] M. K. Eckstein, S. L. Master, R. E. Dahl, L. Wilbrecht, and A. G. Collins. Reinforcement learning and bayesian inference provide complementary models for the unique advantage of adolescents in stochastic reversal. *Developmental Cognitive Neuroscience*, 55:101106, 2022.
- [18] S. Escola, A. Fontanini, D. Katz, and L. Paninski. Hidden markov models for the stimulus-response relationships of multistate neural systems. *Neural computation*, 23(5):1071–1132, 2011.

- [19] N. Eshel, J. Tian, M. Bukwich, and N. Uchida. Dopamine neurons share common response function for reward prediction error. *Nature neuroscience*, 19(3):479–486, 2016.
- [20] C. Findling, N. Chopin, and E. Koechlin. Imprecise neural computations as a source of adaptive behaviour in volatile environments. *Nature Human Behaviour*, 5(1):99–112, 2021.
- [21] Y. Ger, E. Nachmani, L. Wolf, and N. Shahar. Harnessing the flexibility of neural networks to predict dynamic theoretical parameters underlying human choice behavior. *PLOS Computational Biology*, 20(1):e1011678, 2024.
- [22] Y. Ger, M. Shahar, and N. Shahar. Using recurrent neural network to estimate irreducible stochasticity in human choice-behavior. *eLife*, 13, 2024.
- [23] F. Gerber and D. W. Nychka. Fast covariance parameter estimation of spatial gaussian process models using neural networks. *arXiv preprint arXiv:2012.15339*, 2020.
- [24] S. Ghosh, P. Birrell, and D. De Angelis. Sample-efficient neural likelihood-free bayesian inference of implicit hmms. In *International Conference on Artificial Intelligence and Statistics*, pages 4888–4896. PMLR, 2024.
- [25] C. D. Grossman, B. A. Bari, and J. Y. Cohen. Serotonin neurons modulate learning rate through uncertainty. *Current Biology*, 32(3):586–599, 2022.
- [26] K. Katahira and A. Toyama. Revisiting the importance of model fitting for model-based fmri: It does matter in computational psychiatry. *PLoS computational biology*, 17(2):e1008738, 2021.
- [27] I. B. Laboratory, V. Aguillon-Rodriguez, D. Angelaki, H. Bayer, N. Bonacchi, M. Carandini, F. Cazettes, G. Chapuis, A. K. Churchland, Y. Dan, et al. Standardized and reproducible measurement of decision-making in mice. *Elife*, 10:e63711, 2021.
- [28] B. Laeng, S. Sirois, and G. Gredebäck. Pupillometry: A window to the preconscious? *Perspectives on psychological science*, 7(1):18–27, 2012.
- [29] A. Lenzi, J. Bessac, J. Rudi, and M. L. Stein. Neural networks for parameter estimation in intractable models. *Computational Statistics & Data Analysis*, 185:107762, 2023.
- [30] J.-J. Li, C. Shi, L. Li, and A. G. Collins. Dynamic noise estimation: A generalized method for modeling noise fluctuations in decision-making. *Journal of Mathematical Psychology*, 119:102842, 2024.
- [31] J.-M. Lueckmann, J. Boelts, D. Greenberg, P. Goncalves, and J. Macke. Benchmarking simulation-based inference. In *International conference on artificial intelligence and statistics*, pages 343–351. PMLR, 2021.
- [32] K. Miller, M. Eckstein, M. Botvinick, and Z. Kurth-Nelson. Cognitive model discovery via disentangled rnns. *Advances in Neural Information Processing Systems*, 36, 2024.
- [33] I. J. Myung. Tutorial on maximum likelihood estimation. *Journal of mathematical Psychology*, 47(1):90–100, 2003.
- [34] Y. Niv, J. A. Edlund, P. Dayan, and J. P. O’Doherty. Neural prediction errors reveal a risk-sensitive reinforcement-learning process in the human brain. *Journal of Neuroscience*, 32(2):551–562, 2012.
- [35] J. P. O’Doherty, A. Hampton, and H. Kim. Model-based fmri and its application to reward learning and decision making. *Annals of the New York Academy of sciences*, 1104(1):35–53, 2007.
- [36] S. T. Radev, U. K. Mertens, A. Voss, L. Ardizzone, and U. Köthe. Bayesflow: Learning complex stochastic models with invertible neural networks. *IEEE transactions on neural networks and learning systems*, 33(4):1452–1466, 2020.
- [37] M. Rmus, T.-F. Pan, L. Xia, and A. G. Collins. Artificial neural networks for model identification and parameter estimation in computational cognitive models. *PLOS Computational Biology*, 20(5):e1012119, 2024.
- [38] J. Rudi, J. Bessac, and A. Lenzi. Parameter estimation with dense and convolutional neural networks applied to the fitzhugh–nagumo ode. In *Mathematical and Scientific Machine Learning*, pages 781–808. PMLR, 2022.
- [39] M. Sainsbury-Dale, J. Richards, A. Zammit-Mangion, and R. Huser. Neural bayes estimators for irregular spatial data using graph neural networks. *arXiv preprint arXiv:2310.02600*, 2023.

- [40] M. Sainsbury-Dale, A. Zammit-Mangion, and R. Huser. Likelihood-free parameter estimation with neural bayes estimators. *The American Statistician*, 78(1):1–14, 2024.
- [41] L. Schumacher, P.-C. Bürkner, A. Voss, U. Köthe, and S. T. Radev. Neural superstatistics for bayesian estimation of dynamic cognitive models. *Scientific Reports*, 13(1):13778, 2023.
- [42] M. Schuster and K. K. Paliwal. Bidirectional recurrent neural networks. *IEEE transactions on Signal Processing*, 45(11):2673–2681, 1997.
- [43] M. Sensoy, L. Kaplan, and M. Kandemir. Evidential deep learning to quantify classification uncertainty. *Advances in neural information processing systems*, 31, 2018.
- [44] R. S. Sutton and A. G. Barto. *Reinforcement learning: An introduction*. MIT press, 2018.
- [45] R. C. Wilson and A. G. Collins. Ten simple rules for the computational modeling of behavioral data. *Elife*, 8:e49547, 2019.
- [46] C. J. Wu. On the convergence properties of the em algorithm. *The Annals of statistics*, pages 95–103, 1983.
- [47] A. Zammit-Mangion and C. K. Wikle. Deep integro-difference equation models for spatio-temporal forecasting. *Spatial Statistics*, 37:100408, 2020.
- [48] A. Zammit-Mangion, M. Sainsbury-Dale, and R. Huser. Neural methods for amortised parameter inference. *arXiv preprint arXiv:2404.12484*, 2024.
- [49] A. R. Zou, D. E. Muñoz Lopez, S. L. Johnson, and A. G. Collins. Impulsivity relates to multi-trial choice strategy in probabilistic reversal learning. *Frontiers in Psychiatry*, 13:800290, 2022.

Table 1: Summary of four computational cognitive models

Name	# of free θ	Input dimension of ANN	Output dimension of ANN	Tractable
4-P RL	4	\mathbb{R}^2 [action, reward]	\mathbb{R}^1 Q-value	Yes
Meta RL	9	\mathbb{R}^2 [action, reward]	$(\mathbb{R}^1, \mathbb{R}^2)$ (Q-value, attentive state)	Yes
HRL	2	\mathbb{R}^5 [action, reward, 3-d stimuli]	$(\mathbb{R}^1, \mathbb{R}^3)$ (Q-value, chosen cue)	No
GLM-HMM	21	\mathbb{R}^3 [action, reward, 1-d stimuli]	\mathbb{R}^3 attentive state	No

Appendix overview

To help the reader, we provide an overview of the contents covered by the ensuing appendices:

- A. Software
- B. Descriptions of Computational Cognitive Models: including 4-P RL, Meta RL, HRL and GLM-HMM cognitive models used in this work.
- C. Further Experimental Details: including network training, evaluation, likelihood-dependant methods, and real-data experimental details.
- D. Additional Robustness Tests: experiments on model misspecification and trial length variation.
- E. Uncertainty Quantification: example integration with evidential deep learning.

A Software

We used Tensorflow for all neural networks. Code to reproduce results is available at <https://github.com/ti55987/lasenet>

B Descriptions of Computational Cognitive Models

B.1 Four-parameter reinforcement learning model

On each trial t , the four-parameter reinforcement learning model (4P-RL) includes a stickiness parameter κ which captures the tendency to repeat choice from the previous trial:

$$P(a) \propto \exp(\beta Q + \kappa \text{same}(a, a_{t-1})) \quad (8)$$

Once the reward r has been observed, the action values are updated based on 3. In addition, we adopt a counterfactual updating in this model, where the value of the non-chosen action also gets updated on each trial ([17]):

$$\begin{aligned} \delta_{\text{unchosen}} &= (1 - r) - Q_t(1 - a) \\ Q_{t+1}(1 - a) &= Q_t(1 - a) + \alpha \delta_{\text{unchosen}} \end{aligned} \quad (9)$$

Instead of having one learning rate, the model differentiates between positive and negative feedback ([34]), by using different learning rates - α^+ and α^- for updating action values after positive and negative outcomes respectively:

$$Q_{t+1}(a) = \begin{cases} Q_t(a) + \alpha^+ \delta & \text{if } r > 0 \\ Q_t(a) + \alpha^- \delta & \text{if } r \leq 0 \end{cases}$$

The 4P-RL model thus includes four free parameters: positive learning rate (α^+), negative learning rate (α^-), softmax beta (β) and stickiness (κ). All priors of the parameters are: $\mathbf{U}(0, 1)$, except that β is $\mathbf{U}(0, 10)$

B.2 Meta reinforcement learning model with dynamic noise

The meta-learning model in the original paper was implemented from [25]. [30] extends the model with dynamic noise and shows the modified model fitting better with experimental data. The model assumes that a participant has two latent states with time-varying transition probabilities (T_0^1, T_1^0) , which denotes from the random to engaged state and vice versa. In the random state, a decision is made randomly. In the engaged state, on each trial t , a decision is sampled from choice probabilities obtained through a softmax function applied to the action values of the left and right actions with a bias. The probability of left choice is given by:

$$P_t(l) = \frac{1}{1 + \exp(\beta \times (Q_t(r) - Q_t(l)) + bias)} \quad (10)$$

Regardless of the state that a participant is in, once the reward is observed, assuming the left action is chosen, Q-values are updated as follows:

$$Q_{t+1}(l) = Q_t(l) + \alpha_t \cdot \delta_t \cdot (1 - E_t) \quad (11)$$

where α_t is either α_+ or α_- based on positive or negative outcomes, respectively, E_t is an evolving estimate of expected uncertainty calculated from the history of absolute reward prediction errors (RPEs):

$$\begin{aligned} E_{t+1} &= E_t + \alpha_v \cdot v_t \\ v_t &= |\delta_t| - E_t \end{aligned} \quad (12)$$

When RPE is negative, the negative learning rate is dynamically adjusted and lower-bounded by 0:

$$\alpha_{(-)t} = \max(0, \psi \cdot (v_t + \alpha_{(-)0}) + (1 - \psi) \cdot \alpha_{(-)t-1}) \quad (13)$$

Lastly, the unchosen action is forgotten:

$$Q_{t+1}(\text{unchosen action}) = \xi \cdot Q_t(\text{unchosen action}) \quad (14)$$

The model thus has 9 parameters: two transition probabilities (T_0^1, T_1^0) , softmax beta (β), bias (for the right action), positive learning rate (α^+), baseline negative learning rate (α_0^-), learning rate of RPE magnitude integration (α_v), meta-learning rate for unexpected uncertainty (ψ), and forgetting rate (ξ). All priors of the parameters are: $\mathbf{U}(0, 1)$, except that β is $\mathbf{U}(0, 20)$

Note that the likelihood is tractable in Meta RL, because the model assumes that the latent state only affects the policy to choose an action. In the random state, information is thus still being processed (e.g., Q-values updating given rewards) [30].

B.3 Hierarchical reinforcement learning

The hierarchical reinforcement learning (HRL) model follows the similar updating policy as 4-P RL except that the model tracks the values of each arrow-following rule described in 4.3. With N arrows, the complete probability of choosing each arrow is given by:

$$P(\text{arrow}_i) = \frac{\exp(\beta Q_t(\text{arrow}_i))}{\sum_{i=1}^N \exp(\beta Q_t(\text{arrow}_i))} \quad (15)$$

For simplicity, different from 4-P RL, the model has no stickiness κ and has a single shared learning rate for both positive or negative outcomes. The model includes only 2 free parameters: learning rate $\alpha \sim \mathbf{U}(0.4, 0.7)$; and softmax beta $\beta \sim \mathbf{U}(1, 10)$

HRL likelihood is intractable: The likelihood in the HRL model is intractable due to the need to integrate over uncertainty of what rule (which arrow) the participant followed on all of the past trials; because the integration exponentially increases with each trial, the likelihood is not tractable beyond the first several trials T :

$$\begin{aligned} \mathcal{L}(\theta) &= \sum_{t=1}^T \log \mathbb{P}(a_t | h_t, \bar{h}_{t-1}, \theta) \\ &= \sum_{t=1}^T \log \mathbb{P} \left(\sum_c \mathbb{P}(a_t | h_t, \text{rule}_t = c; \theta) \mathbb{P}(\text{rule}_t = c | \bar{h}_{t-1}; \theta) \right) \end{aligned}$$

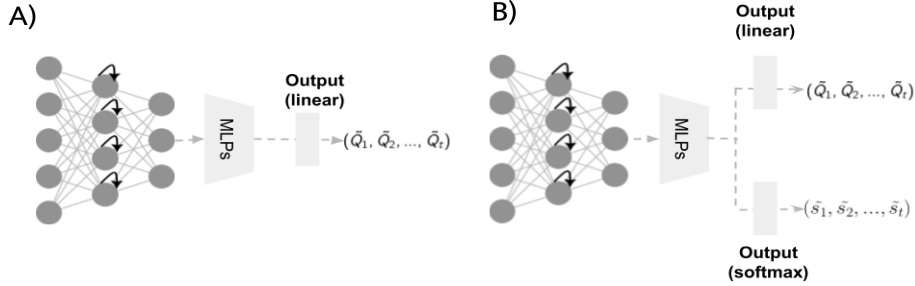


Figure 5: **Network structures** (A) The building blocks of LaseNet consists of one recurrent neural network (RNN) followed by two layers of MLPs. (B) To predict both discrete and continuous latent variables, we add two different output layers but receive the same embeddings from MLPs as input.

Table 2: Hyperparameters selection

Hyperparameter	Sweep range
# of units in RNN layer	U(36, 326)
dropout rate in RNN layer	U(0.05, 0.25)
dropout rate in 1st MLP layer	U(0.01, 0.1)
dropout rate in 2nd MLP layer	U(0.01, 0.05)

where a_t denotes the action a participant chose (left/right), \bar{h}_{t-1} corresponds to the task history encoding rewards, selected actions/sides, arrow directions, and c correspond to identity/color of the correct arrow.

B.4 Hidden Markov Models with Bernoulli generalized linear model observation

We use a framework based on HMMs with Bernoulli generalized linear model (GLM) observations to analyze decision-making behaviors in mice [2]. The resulting GLM-HMM, also known as an input-output HMM, supports an arbitrary number of states that can persist over a large number of trials and have different dependencies on the stimulus and other covariates. A GLM-HMM consists of two basic components: an HMM that governs the distribution across latent states and a set of state-specific GLMs, specifying the strategy employed in each state. For a GLM-HMM with K latent states, the HMM has a $K \times K$ transition matrix A specifying the probability of state transition,

$$P(z_t = k | z_{t-1} = j) = A_{jk} \quad (16)$$

where A_{jk} denotes the transition from state j to state k , z_{t-1} and z_t indicate the latent state at trials $t-1$ and t , respectively. To represent the state-dependent mapping from inputs to decisions, the GLM-HMM comprises K independent GLM weights, each defined by a vector w indicating how inputs are integrated in that particular state (described in Eq 7). We use 4-dimensional w for inputs: stimuli, bias, previous choice, and win-stay/lose-switch. With a three-state GLM-HMM, there are 21 free parameters: $\theta \equiv \{A, w_{k=1}^{k=3}\}$, which A is a 3×3 transition matrix and $w_k \in \mathbb{R}^4$ is a GLM weight vector for state k .

Intractable likelihood Similar to HRL, instead of tracking latent cues, the likelihood is computed by the sum over all possible K hidden states in the T trials. This results in K^T terms as marginalizing all possible paths.

C Further Experimental Details

C.1 Details of Neural Networks Training

All networks trained in this work consisted of one bi-RNN followed by two hidden layers (MLPs). We used rectified linear unit (ReLU) as an activation function in MLPs layers. All the training was performed on Nvidia 676 V100 GPUs with 25 GB memory. The training required between 15 to 45

minutes to complete. Network parameters were randomly initialized and optimized by Adam, with a learning rate of $3 * 10^{-4}$. Each network was trained with at most 600 epochs and a batch size of 128. To avoid overfitting, we used 35 epochs as our early stopping criteria based on the loss in validation data. We fine-tuned hyperparameters with Bayesian optimization algorithms [5] applied on validation data.

We swept values for the hyperparameters with the range summarized in Table 2. We used 10% of the training data as the validation set to fine-tune the hyperparameters. The batch size is fixed to 128 and the learning rate is $3e - 4$ for all the training. The network architecture has a pyramid shape like Fig 5, with decreasing layer width from largest to the output dimension. After the first layer (i.e., bi-RNN layer), the number of units of each layer is the half of the previous layer.

C.2 Evaluation Metrics

Root Mean-squared error RMSE measures the difference between true (z) and predicted latent variables (\hat{z}) from the estimators. We use RMSE to quantify the performance of inferring continuous latent variables (i.e., Q-values). RMSE across trials T is defined as:

$$\text{RMSE}(\mathbf{z}, \hat{\mathbf{z}}) = \sqrt{\frac{1}{T} \sum_{i=1}^T (z_i - \hat{z}_i)^2} \quad (17)$$

Negative log loss NLL measures the predicted probability \mathbf{p} from the estimators based on ground-truth discrete labels. We use NLL to quantify the performance of inferring discrete latent variables (i.e., attentive states and chosen cues). NLL across trials T and a set of M labels is defined as:

$$\text{Log Loss}(\mathbf{z}, \mathbf{p}) = -\frac{1}{T} \sum_{i=1}^T \sum_{j=1}^M z_{ij} \log(p_{ij}) \quad (18)$$

Accuracy We computed the balanced accuracy that avoids inflated performance estimates on imbalanced datasets. It is the macro-average of recall scores per state. Thus for balanced datasets, the score is equal to accuracy. We used balanced accuracy to quantify the performance of inferring discrete latent variables, by taking the state with highest probability as the predicted state. Balanced accuracy is defined as:

$$\text{Balanced Accuracy} = \frac{1}{2} \left(\frac{\text{TP}}{\text{TP} + \text{FN}} + \frac{\text{TN}}{\text{TN} + \text{FP}} \right) \quad (19)$$

where TP is true positive, TN is true negative, FP is false positive, and FN is false negative.

Other than three matrices above, we used coefficient of determination R^2 and Pearson correlation coefficients r to measure the performance of parameter recovery shown in Appendix C.3. R^2 represents the proportion of variance in true parameters that can be explained by a linear regression between true and predicted parameters. Best possible R^2 score is 1. Pearson correlation coefficients r represents the strength of a linear association between true and predicted parameters. Since a positive correlation is desired, the best possible r score is 1.

C.3 Details of Likelihood-dependant Methods

In this appendix, we described in details of using likelihood-dependent method to infer latent variables. The fitting process consists of two steps: identifying the best-fitting parameters and then inferring the latent variables with best-fitting parameters.

C.3.1 Maximum likelihood and Maximum a posteriori estimation

Maximum likelihood estimation (MLE) leverages probability theory and estimation of likelihood $P(Y | \theta)$ of the data given the model parameters and assumptions ([33]). The best fitting parameters are determined by maximizing the log likelihood of the data:

$$\theta_{MLE} = \arg \max_{\theta} P(Y | \theta) = \arg \max_{\theta} \sum_i \log P(y_i | \theta) \quad (20)$$

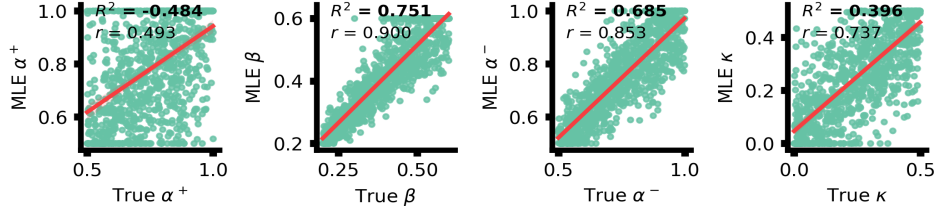


Figure 6: **4-P RL parameters recovered by MLE** R^2 is a R-squared score. r corresponds to Pearson correlation coefficient, red line represents a least squares regression line. High correlation score shows that MLE recovers well in this simple RL model.

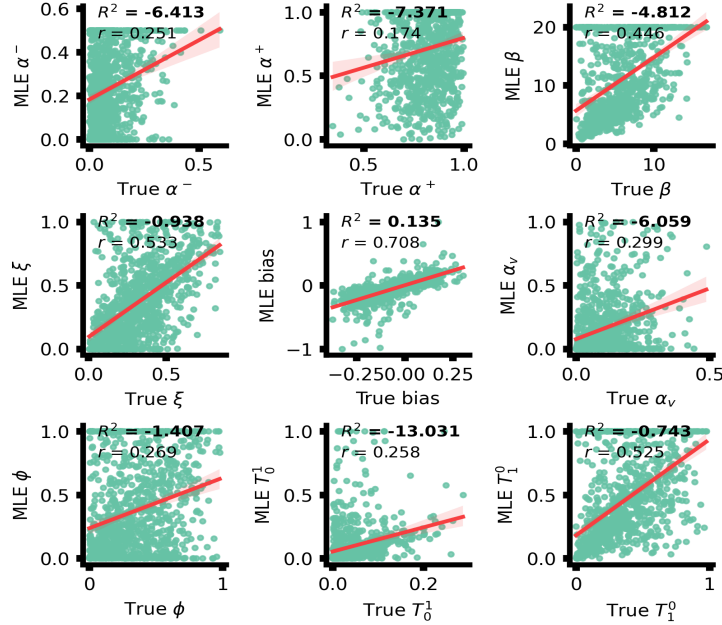


Figure 7: **Meta RL parameters recovered by MLE** Unlike Fig. 6, MLE shows fairly limited parameter recovery in a highly parameterized model, which may impair MLE-dependent latent variable estimation.

To find the parameters via MLE, we used the Sequential Quadratic Programming (SQP) method provided by MATLAB `fmincon`. SQP allows solving the optimization problem with constraints. The constraints we imposed on are the empirical ranges of each model parameters (e.g., $[0, 1]$ for parameters' search space). Fig 6 and Fig 7 shows the recovered parameters in experiments with tractable model 4.2. With the recovered parameters and the observable data Y , we then derived the latent variables such as Q-values by running through the RL functions.

Maximum a posteriori estimation (MAP) relies on the similar principle, with an addition of a prior $P(\theta)$ to maximize the log posterior:

$$\theta_{MAP} = \arg \max_{\theta} \sum_i [\log P(y_i | \theta) + \log P(\theta)] \quad (21)$$

We employed MAP in prior misspecification experiments 4.4 for fitting data generated from a 4-P RL model. Specifically, we tested different β parameter prior (Fig 3, keeping other priors with uniform distributions). Same as MLE, we used the SQP algorithm in MATLAB and derived latent variables with the recovered parameters and the observable data.

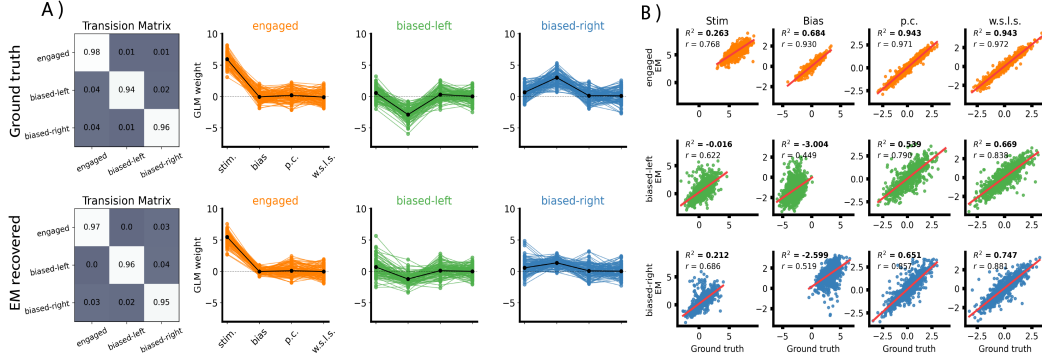


Figure 8: **3 states GLM-HMM recovered by EM** (A) Top row: simulated ground truth of transition matrix and GLM-weights in three states: engaged, biased-left, and biased-right. Bottom row: the well-recovered parameters from EM: high engaged state in the transition matrix, high stimulus GLM weight in engaged state, negative bias weight in left-biased state, and vice versa (GLM takes left as negative; right as positive value). (B) Each row represents GLM weights in three different states and each column represents four weighted features: stimuli, bias, previous choice, win-stay/loss-switch. In GLM-HMM case, we showed that good recovery in parameters doesn't guarantee high precision in latent variables estimation compared to LaseNet (Fig. 2B).

C.3.2 Expectation-Maximization

Expectation-maximization (EM) algorithm is an iterative method for determining the maximum likelihood or maximum a posteriori estimates of parameters in statistical models based on unobserved latent variables Z . The log likelihood to be maximized is thus given by marginalizing out latent variables Z :

$$\log P(Y | \theta) = \sum_z \log P(Y, Z | \theta) \quad (22)$$

Nonetheless, this is intractable in GLM-HMM model as described in B.4. Hence, following the same approach in [2], we maximize the complete log likelihood instead. During the E-step of the EM algorithm, we compute the expected complete data log-likelihood (ECLL), which is a lower bound on Eq. 22. We can derive the lower bound as:

$$\begin{aligned} \log P(Y | \theta) &= \log \sum_z P(Y, Z | \theta) \\ &= \log \sum_z P(Z | Y, \theta) \frac{P(Y, Z | \theta)}{P(Z | Y, \theta)} \\ &= \log \left(\mathbb{E}_{P(Z|Y, \theta)} \left[\frac{P(Y, Z | \theta)}{P(Z | Y, \theta)} \right] \right) \\ &\geq \mathbb{E}_{P(Z|Y, \theta)} \log \left[\frac{P(Y, Z | \theta)}{P(Z | Y, \theta)} \right] \end{aligned}$$

Then, during the 'maximization' or M-step of the algorithm, we maximize the ECLL with respect to the model parameters θ . To understand this iterative algorithm converges to the desired log likelihood, please see [46] for the actual proof.

Fig 8 shows the recovered transition matrix and GLM weights in a three state GLM-HMM model after applying EM. We then infer the most probable latent states by running the E-step with the best-fitting parameters and the input data.

C.4 Infer Latent Variables in Mice Dataset

In this section, we outlined the training details of LaseNet for real mice data.

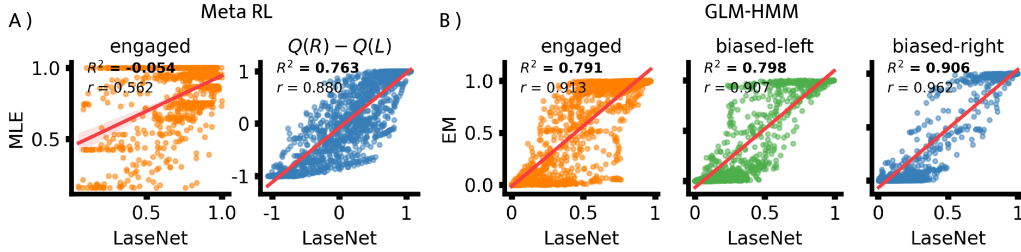


Figure 9: **Correlation between LaseNet and likelihood-dependent methods in real data** (A) In Meta RL, MLE and LaseNet has similar estimated engaged probability and strong correlation in estimated Q-values difference. (B) In GLM-HMM, EM and LaseNet shows high positive correlation in predicting state probability.

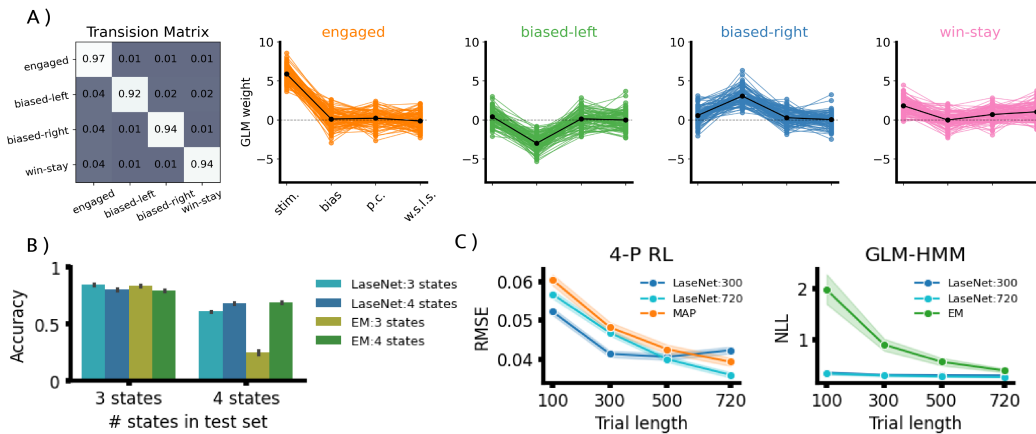


Figure 10: **Robustness Tests** (A) A four state GLM-HMM with additional win-stay state compared to three-state GLM-HMM in Fig. 8. A win-stay has a relatively high win-stay, loss-switch weight in GLM. (B) Accuracy drops when fitting with a wrong model prior in both EM and LaseNet. A model identification is thus needed before inferring the latent states. (C) In both 4-P RL and GLM-HMM, LaseNet trained with longer trials exhibits more robust results across different trial lengths.

Dynamic foraging dataset We first simulated 9000 participants from Meta RL model described in Appendix B.2; each simulated participant has 720 trials. The parameters of Meta RL model were drawn from empirical distribution given by [30]. We then trained LaseNet with the simulated participants; LaseNet takes a time series of rewards and actions as input (Table 1), and outputs three time-varying latent variables: attentive states, Q-values of leftward action, and Q-values of rightward action. Compared to MLE, we found higher correlation in Q-values difference estimation, than latent state probability estimation (Fig. 9A).

IBL dataset We simulated 6000 participants from GLM-HMM model described in B.4; each simulated participant has 500 trials. We used an equal transition probability between states. GLM weights were drawn from empirical distribution given by [2]. We trained LaseNet with simulated participants. LaseNet takes a time series of rewards, actions, and stimuli as input (Table 1), and outputs one latent variable with three possible states: engaged, left-biased and right-biased. Fig. 9B shows high correlation between EM and LaseNet in inferring latent state probabilities.

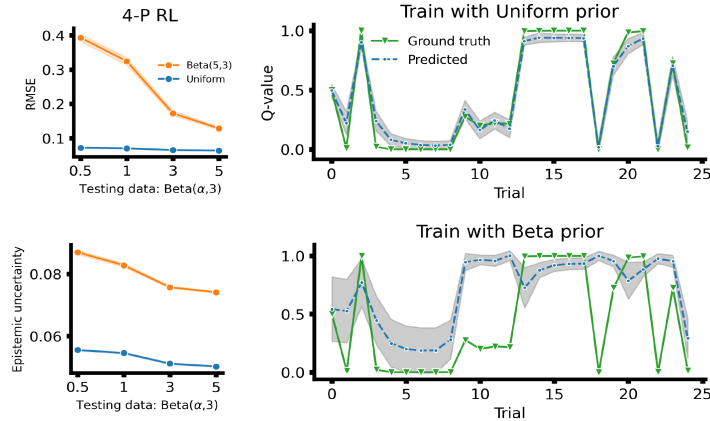


Figure 11: **Uncertainty Quantification in 4-P RL** Two LaseNet estimators: one is trained with a uniform prior and the other is trained with a beta prior (Fig 3A). LaseNet trained with a uniform prior has lower RMSE and uncertainty as testing with unseen data generated from different distributions. In right columns, grey area shows ± 1 standard deviation.

D Additional Robustness Tests

D.1 Model misspecification

We tested model misspecification by fitting data generated from a 3-states GLM-HMM to estimators with a 4-states prior, and vice versa. For LaseNet estimators, we trained two neural networks with data generated from 3 and 4 states priors, respectively. Data generated from a 3-states GLM-HMM has the same model prior as previous experiments (Fig 8A), while data from a 4-states GLM-HMM has the prior shown in Fig 10A. We added a "win-stay" state for a 4-states GLM-HMM based on empirical results in [2]. Each LaseNet estimator was trained with 3000 simulated samples. We generated additional 500 simulated samples for each state priors as test sets. All samples have 720 trials. We compared our trained LaseNet estimators with EM having either 3 or 4 states priors. We found that both EM and LaseNet have lower accuracy when fitting with misspecified models (Fig 10B). Hence, model identification should be performed before inferring latent states.

D.2 Trial length variation

We examined LaseNet in inferring latent states with different trial's lengths, because in real experiments, researchers commonly collect varying trial's lengths. We tested two cognitive models, 4-P RL and GLH-HMM, with four different trial's lengths: 100, 300, 500, and 720. In comparison to likelihood-dependent methods, we trained two LaseNet estimators with data generated from 300 and 720 trials, respectively. Each LaseNet estimator was trained with 22000 simulated samples for 4-P RL and with 9000 simulated samples for GLM-HMM. For testing, we generated additional 500 simulated samples for each trial length. Fig 10B shows that training with 720 trials reaches higher precision consistently across all trial lengths compared to likelihood-dependent methods. Note that EM is susceptible to a short trial length because we can only approximate likelihood for GLM-HMM as described in C.3.2; shorter trial length yields less data points for approximation.

E Uncertainty Quantification

In this appendix, we explored the potential of integrating with evidential deep learning [1, 43]. Evidential deep learning aims to train a neural network to learn a higher-order, evidential distribution and then output the hyperparameters of the evidential distribution. Here, we adopted the loss functions proposed in [1] to quantify the uncertainty for inferring Q-values in a 4-P RL model. The network structure is the same as Fig 5 except that the objective function is maximizing and regularizing evidence. To measure the effect of evidential deep learning, we compared two LaseNet

estimators trained with different β model priors: uniform and beta distribution, illustrated in Fig 3A. Each LaseNet estimator was trained using 3000 simulated samples, each consisting of 500 trials. Fig 11 shows that the LaseNet estimator trained with a uniform prior exhibits lower RMSE and uncertainty. Higher uncertainty also corresponds to higher RMSE. Our implementation is extended from: <https://github.com/aamini/evidential-deep-learning>